# Restora-Flow: Mask-Guided Image Restoration with Flow Matching

Arnela Hadzic<sup>1</sup>, Franz Thaler<sup>1,2,3</sup>, Lea Bogensperger<sup>4</sup>, Simon Johannes Joham<sup>1</sup>, Martin Urschler<sup>1</sup>

<sup>1</sup>Institute for Medical Informatics, Statistics and Documentation, Medical University of Graz, Graz, Austria 
<sup>2</sup>Division of Medical Physics and Biophysics, Medical University of Graz, Graz, Austria 
<sup>3</sup>Institute of Visual Computing, Technical University of Graz, Graz, Austria 
<sup>4</sup>Department of Quantitative Biomedicine, University of Zurich, Zurich, Switzerland

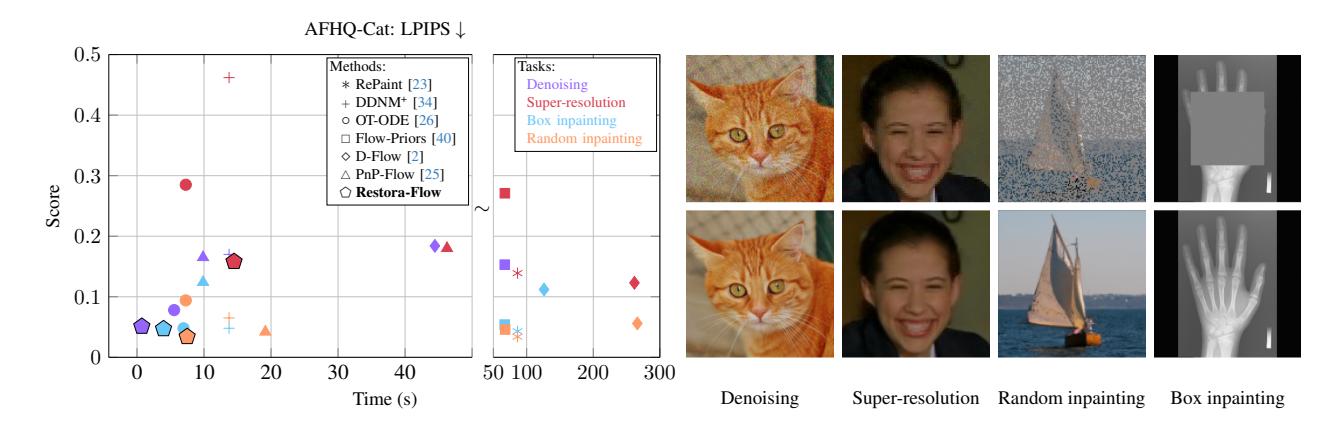


Figure 1. We propose **Restora-Flow**, a mask-guided image **restora**tion method based on **flow** matching with an integrated trajectory correction mechanism. Restora-Flow offers excellent performance in both reconstruction quality and processing efficiency when compared to state-of-the-art methods for various tasks. This is demonstrated in the results showing LPIPS perceptual quality score vs. processing time for the AFHQ-Cat dataset (left). Exemplary qualitative reconstruction results of Restora-Flow are shown across four different tasks and evaluated on four datasets with distinct characteristics (right).

## **Abstract**

Flow matching has emerged as a promising generative approach that addresses the lengthy sampling times associated with state-of-the-art diffusion models and enables a more flexible trajectory design, while maintaining highquality image generation. This capability makes it suitable as a generative prior for image restoration tasks. Although current methods leveraging flow models have shown promising results in restoration, some still suffer from long processing times or produce over-smoothed results. To address these challenges, we introduce Restora-Flow, a training-free method that guides flow matching sampling by a degradation mask and incorporates a trajectory correction mechanism to enforce consistency with degraded inputs. We evaluate our approach on both natural and medical datasets across several image restoration tasks involving a mask-based degradation, i.e., inpainting, superresolution and denoising. We show superior perceptual

quality and processing time compared to diffusion and flow matching-based reference methods. Code is available at https://github.com/imigraz/Restora-Flow.

## 1. Introduction

Many important image restoration tasks, such as image denoising, super-resolution and inpainting, can be framed as inverse problems involving mask-based degradation. The objective is to recover an original image  $x \in \mathbb{R}^d$  from its degraded observation  $z = Hx + \xi$ , where H represents a degradation operator using a mask m, and  $\xi \sim \mathcal{N}(0, \sigma^2 I)$  denotes measurement noise. The goal of image restoration is twofold: the restored image should exhibit high visual quality while also maintaining fidelity to the input data, ensuring consistency with the degraded observation.

Over the last few years, diffusion models have become a standard approach for generative modeling due to their ability to learn complex data distributions and generate high-quality images [8, 15, 27, 28, 31]. This has led to a growing interest in utilizing these generative models as unsupervised priors in inverse problems [7], with numerous successful applications to guide the restoration process [6, 17, 18, 23, 24, 29, 34, 41]. However, a significant limitation of these methods is the long sampling time due to highly curved sampling trajectories [1], as well as the inherent challenges arising from the intermediate noisy steps.

More recently, Flow Matching (FM) has emerged as an alternative approach in generative modeling [20, 21], characterized by its ability to maintain significantly straighter trajectories during data generation compared to diffusion models. FM defines the generative process using conditional optimal transport paths through Ordinary Differential Equations (ODEs). Recent research shows that FM achieves faster training and sampling while still generating high-quality images [4, 12, 37], making it a promising direction for addressing image restoration tasks. To date, only a few studies have investigated the use of flow-based priors in solving image restoration [2, 25, 26, 40]. While these studies show promising results, some still suffer from relatively long processing times [2, 40], others yield oversmoothed samples [25], or tend to produce artifacts [26].

In this work, we introduce Restora-Flow, a training-free, flow matching-based approach, specifically designed to address mask-based image restoration tasks. Our approach conditions the sampling process of an unconditional flow matching model through mask-guided fusion, ensuring that regions unaffected by the degradation operator H are preserved during sampling. The samples are then refined using a trajectory correction mechanism to enforce consistency with degraded observations. When evaluated on several image restoration tasks using various datasets, Restora-Flow achieves the new state-of-the-art when simultaneously assessing both reconstruction quality and processing time. Our contributions are summarized as follows:

- We introduce Restora-Flow, a training-free algorithm for addressing mask-based inverse problems, utilizing unconditional flow prior models and mask-guided fusion for flow matching sampling.
- To enhance fidelity of the restoration process, we introduce a novel correction mechanism that guides the flow trajectory toward better alignment with observed data.
- We perform a comprehensive evaluation using computer vision and medical datasets across various settings for inpainting, super-resolution and denoising tasks. The results show that our method achieves superior perceptual quality compared to related approaches [2, 25, 26, 40], while also demonstrating the fastest processing time.

### 2. Related Work

With the advent of deep learning, deep neural networks have become widely utilized in image restoration tasks. Various methods have been proposed to learn a direct mapping from degraded measurements to clean images by minimizing a reconstruction loss [9, 32, 35, 38]. However, these approaches typically require datasets containing paired degraded and clean images and necessitate retraining for each new task. To overcome these limitations, recent research has investigated the use of deep generative priors, such as diffusion or flow matching-based priors, due to their ability to model complex data statistics [16, 30]. These generative approaches do not rely on paired datasets, enabling their application across various different image restoration tasks using the same prior knowledge.

Several diffusion-based approaches for image restoration have introduced guidance strategies to ensure consistency with degraded observations during the generation process. DDRM [18] tackles linear inverse problems by employing singular value decomposition of the degradation operator H. Similarly, DDNM<sup>+</sup> [34] addresses inverse problems in a zero-shot manner by utilizing range-null space decomposition as the guidance function, whereas RePaint [23] uses unmasked regions to guide the diffusion process for inpainting tasks. To ensure consistency between denoising results and degraded measurements,  $\Pi$ GDM [29] incorporates a vector-Jacobian product as additional guidance. In contrast, RED-Diff [24] formulates image restoration as an optimization problem, minimizing a measurement consistency loss while applying score-matching regularization.

More recently, the application of flow matching as a prior in image restoration has gained considerable attention. OT-ODE [26] incorporates the gradient correction term from IIGDM to guide the flow-based generation process. Their findings demonstrate that images restored using flow matching priors have superior perceptual quality compared to those generated via diffusion paths, as well as those produced by RED-Diff or IIGDM. Similarly to RED-Diff, D-Flow [2] formulates the image restoration process as a source point optimization problem. The objective is to minimize the cost function associated with the initial point in the flow matching framework. However, this optimization requires backpropagation through an ODE solver, resulting in relatively long sampling times (i.e., 5 to 15 minutes per sample, as reported in [2]). In contrast, Flow-Priors [40] decomposes the flow's trajectory into several local objectives and employs Tweedie's formula [11] to sequentially optimize these objectives through gradient steps, resulting in reduced sampling time compared to D-Flow. Instead, PnP-Flow [25] combines Plug-and-Play methods [33] with flow matching without requiring backpropagation, however, it tends to produce over-smoothed results.

### 3. Method

We introduce Restora-Flow, a novel training-free method for mask-based image restoration that leverages flow matching generative priors. At its core, Restora-Flow performs time-dependent ODE-based sampling guided by a mask and employs a trajectory correction mechanism that refines the generative path toward the data manifold. This correction is designed to align the evolving sample with the degraded input, thereby improving consistency between restored and observed known regions. Empirically, we find that a single correction step per ODE iteration is sufficient to ensure this consistency, enabling both high reconstruction quality and fast processing times (see Figs. 1 and 2).

### 3.1. Flow Matching (FM)

In flow matching [20, 21], the idea is to learn a velocity field  $v_{\theta,t}$  of the probability flow  $\Psi_t$ . This field governs the transformation of a simple base distribution at t=0 into the target distribution p(x) at t=1 by defining a continuous-time trajectory that maps between them. For simulation-free training, the conditional FM loss [20] is used:

$$\min_{\theta} \mathbb{E}_{t,x_1,x_0} \left[ \frac{1}{2} \left\| v_{\theta,t}(\Psi_t(x_0)) - (x_1 - x_0) \right\|^2 \right], \quad (1)$$

with  $t \sim \mathcal{U}[0,1], x_1 \sim \mathrm{p}(x), x_0 \sim \mathcal{N}(0,I)$ , and the conditional flow  $\Psi_t(x_0) = (1-t)x_0 + t\,x_1$ . The learned vector field  $v_{\theta,t}$  models the distribution's change in time, from which we can sample by integrating the corresponding ODE:

$$\frac{\mathrm{d}}{\mathrm{d}t}\Psi_t(x) = v_{\theta,t}(\Psi_t(x)). \tag{2}$$

For example, using the explicit Euler integration scheme with  $t = 0, \dots, 1 - \Delta_t$ , the estimate is updated via

$$x_{t+\Delta_t} = x_t + \Delta_t \, v_{\theta,t}(x_t). \tag{3}$$

## 3.2. Restora-Flow Algorithm

The restoration of an unknown image x from its degraded observation z can be formulated as a maximum a posteriori (MAP) estimation problem:

$$\hat{x} = \arg\min_{x} \mathcal{D}(Hx, z) + \mathcal{R}_{\theta}(x), \tag{4}$$

where H is the degradation operator,  $\mathcal{D}(Hx,z)$  is a data fidelity term, and  $R_{\theta}(x)$  is a prior encoding learned prior knowledge about images, parameterized by  $\theta$ .

When employing flow matching as the prior  $\mathcal{R}_{\theta}(x)$ , the generation of samples via only Eq. (3) does not yield a minimizer of Eq. (4). Therefore, the sampling must be guided toward the MAP solution by incorporating the degraded observation z into the sampling process. To optimize Eq. (4), one can use either explicit gradient steps on the data term  $\nabla_x \mathcal{D}(Hx,z)$  or implicit strategies, such as mask-guided update used in inpainting [23]. We opt for mask-guidance, due to its inherent relationship with inpainting and other image restoration tasks involving mask-based degradations.

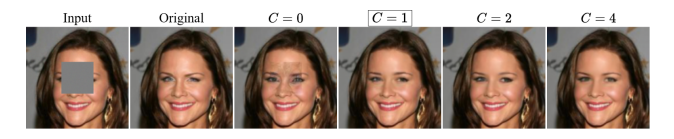


Figure 2. Restora-Flow samples with and without correction steps. Empirically, one correction step (C=1) offers the best trade-off between high reconstruction quality and fast processing.

**Incorporating mask-guidance** Mask-guidance, introduced by RePaint [23], fuses the time-dependent variable  $x_t$  with the unmasked portion of the original image z. First, z is adapted to match the noise level contained in the flow estimate  $x_t$  through the convex combination

$$z' = tz + (1 - t)\epsilon, \quad \epsilon \sim \mathcal{N}(0, I),$$
 (5)

and is subsequently fused with  $x_t$  via

$$x_t' = m \odot z' + (1 - m) \odot x_t, \tag{6}$$

where  $\odot$  denotes element-wise multiplication and m is a binary mask indicating known and unknown regions in z.

A naive way to use the mask-based guidance in flow matching is to fuse each time-dependent sample  $x_t$  before the flow matching update (Eq. (3)). This yields a modified update equation

$$x_{t+\Delta_t} = x_t' + \Delta_t v_{\theta,t}(x_t'), \tag{7}$$

where  $x_t'$  is the sample fused according to Eq. (6). However, this approach leads to visible misalignments between known and unknown regions in the updated samples  $x_{t+\Delta_t}$ , particularly at mask boundaries. Thus, the distribution of fused samples diverges from the flow matching model training distribution. In other words, in this naive strategy,  $x_t'$  is unlikely to lie on a trajectory consistent with the learned generative process. Consequently, the flow matching model cannot be relied on to map  $x_t'$  to a high-quality image.

**Trajectory correction** To address this issue and improve the quality of generated samples, we introduce a trajectory correction mechanism. After the initial mask-guided update (Eq. (7)), we perform a forward extrapolation using the learned velocity field to project the sample toward the endpoint at t=1 of the generative path:

$$\widetilde{x}_1 = x_{t+\Delta_t} + (1 - (t + \Delta_t)) v_{\theta,t+\Delta_t}(x_{t+\Delta_t}). \tag{8}$$

This extrapolation acts as a learned denoiser, helping to project the sample closer to the data manifold and correct misalignments caused by the mask fusion.

To place the sample at the correct location along the generative trajectory, we scale the extrapolated sample and reintroduce noise:

$$x_t = t\widetilde{x}_1 + (1 - t)\eta, \quad \eta \sim \mathcal{N}(0, I).$$
 (9)

This reintroduction of noise adds stochasticity back into the generative process, allowing the flow model to generate diverse and realistic images.

Repeated application of this correction enhances consistency with the known input while allowing the unknown regions to evolve naturally under the flow matching prior. Empirically, we find that even a single correction per ODE step significantly improves the alignment between the restored and observed content (see Fig. 2).

#### Algorithm 1 Mask-Guided Restora-Flow Sampling

```
1: Input: learned flow network v_{\theta}, degraded observation
     z \in \mathbb{R}^d, number of ODE steps N (with \Delta_t \leftarrow \frac{1}{N}),
     number of corrections C > 0, mask m
 2: Sample x \sim \mathcal{N}(0, I)
 3: for t = 0, \Delta_t, \dots, 1 - \Delta_t do
 4:
          for c = 0, \ldots, C do
                Sample \epsilon \sim \mathcal{N}(0, I)
 5:
                z' \leftarrow tz + (1-t)\epsilon if t > 0, else z' = 0
 6:
                x' \leftarrow m \odot z' + (1 - m) \odot x
 7:
                x \leftarrow x' + \Delta_t v_{\theta,t}(x',t)
 8:
 9:
                if c > 0 and t < 1 - \Delta_t then
                      Sample \eta \sim \mathcal{N}(0, I)
10:
                     \widetilde{x}_1 \leftarrow x + (1 - (t + \Delta_t)) v_{\theta, t + \Delta_t}(x, t + \Delta_t)
11:
                     x \leftarrow t\widetilde{x}_1 + (1-t)\eta
12:
                else
13:
                     t \leftarrow t + \Delta_t
14:
15: return x
```

# Algorithm 2 Restora-Flow Sampling for Denoising

```
1: Input: degraded observation z \in \mathbb{R}^d with noise level \sigma, number of ODE steps N (with \Delta_t \leftarrow \frac{1}{N})
2: Sample x_0 \sim \mathcal{N}(0,I)
3: for t = 0, \Delta_t, \dots, 1 - \Delta_t do
4: Sample \epsilon \sim \mathcal{N}(0,I)
5: z' \leftarrow (1-\sigma)z
6: x'_{t+\Delta_t} \leftarrow x_t + \Delta_t v_{\theta,t}(x_t)
7: x_{t+\Delta_t} \leftarrow 1_{\{t < 1-\sigma\}}z' + 1_{\{t \ge 1-\sigma\}}x'_{t+\Delta_t}
8: return x_1
```

Restora-Flow is summarized in Algorithm 1 for mask-based image restoration tasks, such as inpainting and super-resolution. The unconditional sampling process is guided by evolving the sample according to the flow matching prior and applying the mask-guided fusion to incorporate the information of the degraded observation z. This is followed by our proposed correction mechanism for enhanced alignment between generated content and the observation z.

Algorithm 2 describes Restora-Flow for image denoising. In contrast to Algorithm 1, a time-dependent and global mask m(t) is used here where we set m(t) = 1 if  $t < 1 - \sigma$ ,

else it is 0, as given by the indicator function in Algorithm 2. Thus, the noisy observation z is used only as an initialization for the sampling process, and for  $t \geq 1 - \sigma$  the ODE evolves the solution without further influence from z.

## 4. Experimental Setup

**Datasets.** To assess the performance of Restora-Flow, we utilize four datasets: (1) CelebA [22], featuring 162k training images of celebrity faces resized to  $128 \times 128$  pixels; (2) AFHQ-Cat [5], which includes 5k training images of cat faces resized to  $256 \times 256$  pixels; (3) COCO [19], containing 118k training images of various object types resized to  $128 \times 128$  pixels; and (4) X-ray Hand [13, 36], comprising 895 hand radiographs resized to  $256 \times 256$  pixels. In line with recent work [25], we report results on the same 100 test images from the CelebA dataset and on the same 100 test images from the AFHQ-Cat dataset. Moreover, we report results on 100 validation images from the COCO dataset and 298 test images from the medical X-ray Hand dataset.

Tasks. We report results for denoising, box inpainting, super-resolution and random inpainting. Additionally, we include results for a clinically motivated occlusion removal task on the X-ray Hand dataset. All experiments, unless otherwise noted, include a Gaussian measurement noise level of  $\sigma = 0.01$ . For the CelebA and COCO datasets, we employ denoising with a noise level of  $\sigma = 0.2$ , box inpainting with a  $40 \times 40$  centered mask,  $2 \times$  super-resolution, and random inpainting with a mask covering 70% of the pixels. For the AFHQ-Cat dataset, we perform denoising with a noise level of  $\sigma = 0.2$ , box inpainting using an  $80 \times 80$ centered mask, 4× super-resolution, and random inpainting with a mask covering 70% of the pixels. For the X-ray Hand dataset, we employ denoising with  $\sigma = 0.08$ , box inpainting with a  $128 \times 128$  centered mask, and  $2 \times$  superresolution. For occlusion removal, we synthetically add occlusions to images as described in [14].

Baselines and Metrics. We compare Restora-Flow with four flow-based baselines: OT-ODE [26], Flow-Priors [40], D-Flow [2] and PnP-Flow [25] (see Sec. 2). In our experiments on CelebA and AFHQ-Cat, we adopt the hyperparameter values defined in [25], where a grid search was performed to identify optimal settings for each baseline on the respective datasets. Specifically, OT-ODE, Flow-Priors and PnP-Flow each require tuning two hyperparameters, while Flow-Priors requires tuning three hyperparameters, with different values chosen based on the task and dataset. For the COCO dataset, we use the same hyperparameters as for CelebA. For the X-ray Hand dataset, we adopt the same hyperparameters as those used for AFHQ-Cat.

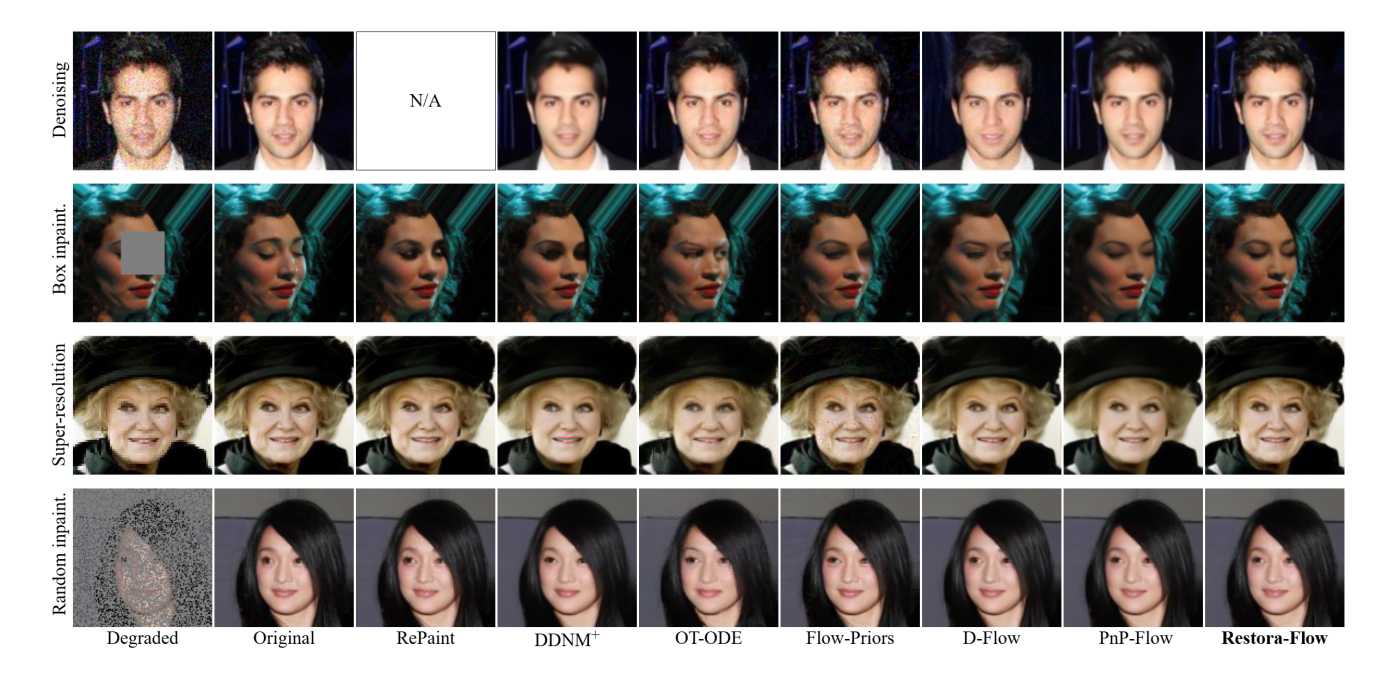


Figure 3. Qualitative results on CelebA. Shown are the degraded image (col 1), original image (col 2), restored images using related work as indicated (cols 3-8) and restored image of Restora-Flow (col 9). Rows refer to denoising (row 1), box inpainting (row 2), super-resolution (row 3) and random inpainting (row 4). RePaint is not applicable to denoising (N/A). Differences can be best seen in the pdf version.

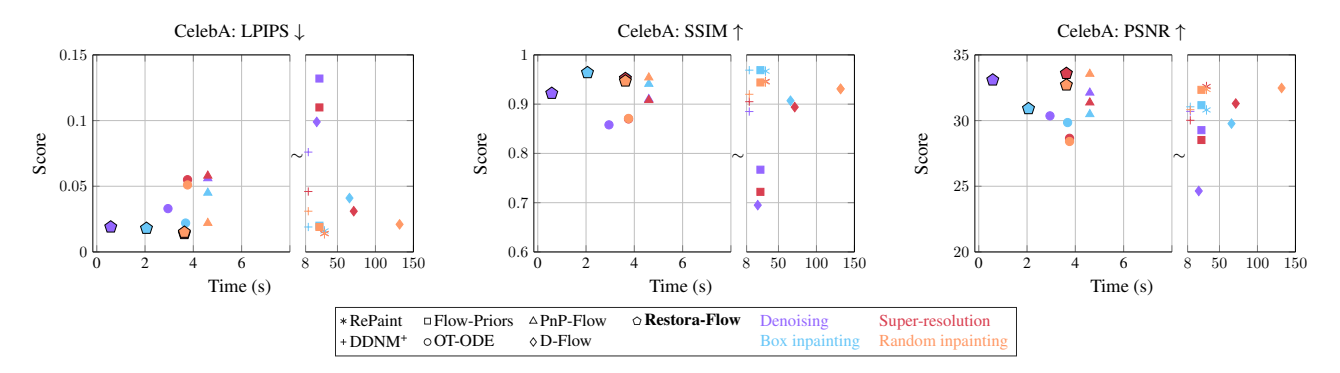


Figure 4. Visual representation of quantitative results on CelebA. Restora-Flow  $(\bigcirc)$  is compared to related work methods (other shapes) on four different tasks (colors). The plots show LPIPS  $\downarrow$  (left), SSIM  $\uparrow$  (center) and PSNR  $\uparrow$  (right) on the y-axis, and processing time  $\downarrow$  (all plots) on the x-axis. For better visualization and comparison, each plot is separated into two parts with different scales in the x-axis.

Furthermore, we compare Restora-Flow with diffusion-based methods, *i.e.*, RePaint [23] and DDNM<sup>+</sup> [34]. For RePaint, we use their proposed hyperparameter values [23]: a jump length of 10 and 10 resampling steps. For DDNM<sup>+</sup>, we achieved optimal performance using the time-travel trick [23, 34] parameters s=1 and l=5.

Following prior work [2, 25, 26, 40], we utilize pixel-based Structural Similarity Index (SSIM) and Peak Signal-to-Noise Ratio (PSNR) as distortion metrics. Given the inherent perception-distortion trade-off [3], we also include Learned Perceptual Image Patch Similarity (LPIPS) [39] as perceptual metric. Furthermore, we report processing time in seconds to restore a single image.

Implementation details. We utilize the pretrained flow-based CelebA and AFHQ-Cat models provided by [25]. To enable a fair comparison with the diffusion-based Re-Paint [23] and DDNM $^+$  [34] methods, we train DDPMs from scratch using the same U-Net architecture and training parameters as the pretrained flow-based models. Specifically, for CelebA, we use a learning rate of 1e-4, a batch size of 128, and train for 200 epochs. For AFHQ-Cat, we use the same learning rate, a batch size of 64, and train for 400 epochs. The number of diffusion time steps is set to 250 for both models. Additionally, we train a DDPM and a flow-based model from scratch on COCO, using a learning rate of 1e-4, a batch size of 64, and a total of 300

Table 1. Quantitative results on CelebA, AFHQ-Cat, COCO and X-ray Hand (from top to bottom). Shown are LPIPS  $\downarrow$ , SSIM  $\uparrow$ , PSNR  $\uparrow$  and processing time  $\downarrow$  for denoising, box inpainting, super-resolution and random inpainting. For X-ray Hand, random inpainting is replaced by occlusion removal. Restora-Flow is compared to several state-of-the-art methods. Best and second best scores are highlighted using bold or underline, respectively. RePaint is not applicable to denoising (N/A).

							CelebA									
Model	Denoising $\sigma = 0.2$			Time	e Box inpainting $40 \times 40$			Time	Super-resolution 2×			Time	e Random inpainting 70%			Time
	LPIPS	SSIM	PSNR	in s	LPIPS	SSIM	PSNR	in s	LPIPS	SSIM	PSNR	in s	LPIPS	SSIM	PSNR	in s
RePaint [23]	N/A	N/A	N/A	N/A	0.016	0.967	30.81	32.89	0.014	0.946	32.59	32.89	0.014	0.945	32.37	32.89
DDNM <sup>+</sup> [34]	0.076	0.885	30.70	11.57	0.019	0.969	31.05	11.57	0.046	0.905	30.02	11.57	0.031	0.920	30.83	11.57
OT-ODE [26]	0.033	0.858	30.36	2.95	0.022	0.954	29.85	3.68	0.055	0.870	28.65	3.76	0.051	0.871	28.41	3.76
Flow-Priors [40]	0.132	0.767	29.27	26.22	0.020	0.969	31.17	26.22	0.110	0.722	28.52	26.22	0.019	0.944	32.34	26.22
D-Flow [2]	0.099	0.695	24.64	22.73	0.041	0.907	29.77	65.81	0.031	0.894	31.30	71.43	0.021	0.931	32.48	131.78
PnP-Flow [25]	0.056	0.910	32.12	4.60	0.045	0.941	30.48	4.60	0.058	0.908	31.37	4.60	0.022	0.954	33.55	4.60
Restora-Flow	0.019	0.922	33.09	0.58	0.018	0.964	30.91	2.06	0.014	0.952	33.59	3.63	0.015	0.947	<u>32.71</u>	3.63
						A	AFHQ-Ca	t								
Denoising $\sigma = 0.2$				Time				Time	Super-resolution 4×			Time	Random inpainting 70%			Time
Model	LPIPS	SSIM	PSNR	in s	LPIPS	SSIM	PSNR	in s	LPIPS	SSIM	PSNR	in s	LPIPS	SSIM	PSNR	in s
RePaint [23]	N/A	N/A	N/A	N/A	0.043	0.939	26.26	86.23	0.139	0.701	24.71	86.23	0.034	0.897	30.93	86.23
DDNM <sup>+</sup> [34]	0.170	0.818	29.06	13.74	0.048	0.942	25.16	13.74	0.462	0.534	19.69	13.74	0.065	0.876	30.12	13.74
OT-ODE [26]	0.078	0.814	29.73	5.54	0.048	0.924	24.36	6.94	0.285	0.565	21.85	7.28	0.094	0.839	28.87	7.28
Flow-Priors [40]	0.153	0.771	29.43	67.10	0.054	0.942	26.04	67.05	0.271	0.565	23.50	67.30	0.046	0.909	31.82	67.69
D-Flow [2]	0.184	0.648	24.98	44.45	0.112	0.839	26.17	126.09	0.123	0.707	25.34	261.84	0.056	0.878	30.97	266.18
PnP-Flow [25]	0.165	0.864	31.10	9.86	0.124	0.904	26.18	9.86	0.180	0.790	26.95	46.26	0.042	0.930	33.07	19.15
Restora-Flow	0.051	0.899	32.35	0.72	0.047	0.939	25.96	3.96	0.158	0.761	26.33	14.48	0.034	0.914	31.99	7.48
							сосо									
	Denc	Denoising $\sigma = 0.2$		Time				Time	Super	r recolutio	n 2 ×	Time	Pandor	Time		
Model	LPIPS SSIM PSNR		in s	LPIPS SSIM PSNR		in s	Super-resolution 2× LPIPS SSIM PSNR		in s	Random inpainting 70% LPIPS SSIM PSNR		in s				
RePaint [23]	N/A	N/A	N/A	N/A	0.093	0.922	21.20	32.89	0.046	0.856	25.84	32.89	0.038	0.876	26.82	32.89
DDNM <sup>+</sup> [34]	0.162	0.805	27.04	11.57	0.033	0.925	21.71	11.57	0.257	0.682	19.05	11.57	0.069	0.845	25.80	11.57
OT-ODE [26]	0.066	0.810	27.52	2.95	0.073	0.914	23.40	3.68	0.146	0.745	23.83	3.76	0.130	0.763	23.98	3.76
Flow-Priors [40]	0.116	0.751	27.08	26.22	0.084	0.927	23.58	26.22	0.112	0.698	24.93	26.22	0.055	0.855	25.97	26.22
D-Flow [2]	0.252	0.552	21.19	22.73	$\frac{0.001}{0.115}$	0.825	23.46	65.81	0.083	0.778	24.80	71.43	0.053	0.840	26.29	131.78
PnP-Flow [25]	0.128	0.855	28.97	4.60	0.121	0.892	24.56	4.60	0.118	0.827	26.73	4.60	0.053	0.896	28.13	4.60
Restora-Flow	0.026	0.905	30.57	0.58	0.084	0.929	24.80	2.06	0.044	0.877	27.44	3.63	0.040	0.881	27.37	3.63
	Danie		0.00	Time	D:		-ray Han	d Time	C	r-resolutio	0.4	Time	01	usion ren	1	Time
Model	LPIPS	ising $\sigma =$ SSIM	PSNR	in s	LPIPS	ainting 1 SSIM	28 × 128 PSNR	in s	LPIPS	SSIM	PSNR	in s	LPIPS	SSIM	PSNR	in s
RePaint [23]	N/A	N/A	N/A	N/A	0.046	0.821	23.90	17.02	0.074	0.767	20.04	17.02	0.032	0.898	29.66	17.02
			23.78	13.35	0.059	0.801	22.76	13.35	0.143	0.635	14.10	13.35	0.047	0.884	26.57	13.35
DDNM <sup>+</sup> [34]	0.057	0.819	43.70													
DDNM <sup>+</sup> [34]	I						23.58		0.076	0.684	22.01	11.17	0.029	0.845	26.55	11.17
	0.057 0.026 0.033	0.819 0.853 0.885	27.83 28.58	8.73 68.54	0.038 0.035	0.801 <b>0.882</b>	23.58 <b>25.74</b>	11.17 68.59	0.076 0.162	0.684 0.460	22.01 20.38	$\frac{11.17}{68.62}$	0.029 0.023	0.845 0.933		11.17 68.59
DDNM <sup>+</sup> [34] OT-ODE [26]	0.026	0.853	27.83	8.73	0.038	0.801		<u>11.17</u>							26.55	
DDNM <sup>+</sup> [34] OT-ODE [26] Flow-Priors [40]	0.026 0.033	0.853 0.885	27.83 28.58	$\frac{8.73}{68.54}$	$\frac{0.038}{0.035}$	0.801 <b>0.882</b>	25.74	$\frac{11.17}{68.59}$	0.162	0.460	20.38	68.62	0.023	0.933	26.55 27.07	68.59

epochs. We use the implementations provided by [25] for all flow-based reference methods. For a fair comparison, we integrate RePaint, DDNM<sup>+</sup> and our proposed method, Restora-Flow, within this framework. Regarding the medical X-ray Hand dataset, we use the pretrained flow-based and diffusion-based models from [14] and implement all baselines and our proposed Restora-Flow within the MED-DDPM framework [10, 14].

For our proposed method Restora-Flow, we use the same number of corrections (i.e., C=1, see Fig. 2), across all experiments and datasets, resulting in only one hyperparameter to optimize: the number of ODE steps (see our ablation in Fig. 5). For all natural image datasets, we apply 64 ODE steps for denoising and box inpainting, 128 ODE steps for  $2\times$  super-resolution and random inpainting, and 256 ODE steps for  $4\times$  super-resolution. For the medical X-

ray Hand dataset, we use 64 ODE steps for denoising and  $2\times$  super-resolution, and 32 ODE steps for box inpainting and occlusion removal. We trained generative prior models on NVIDIA A100 GPUs, which were also utilized for restoration experiments at  $256\times256$  resolution. Experiments at  $128\times128$  resolution were conducted using an NVIDIA GeForce RTX 3090.

## 5. Results

We evaluate the proposed Restora-Flow method by comparing it to related work: quantitatively on all datasets in Tab. 1 and qualitatively on CelebA in Fig. 3 and AFHQ-Cat in Fig. 6. Qualitative results for COCO and X-ray Hand are provided in the supplemental material. Plots visualizing reconstruction quality over processing time per metric of

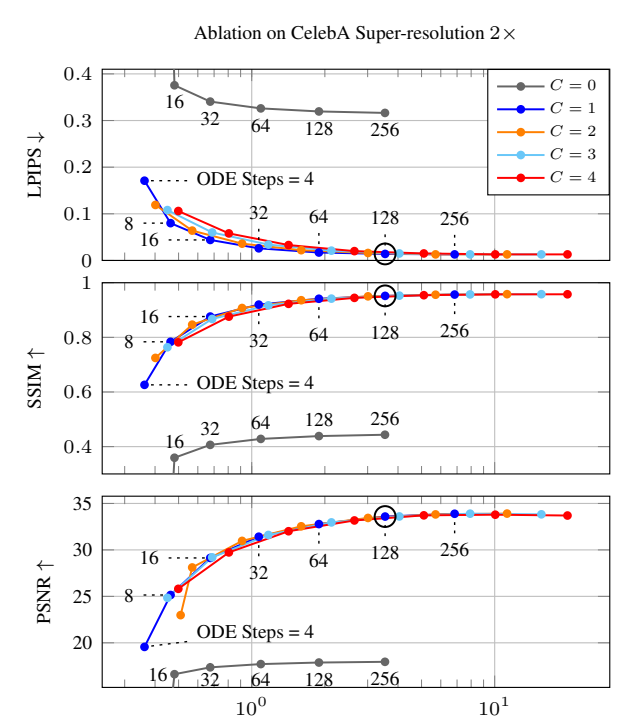


Figure 5. Ablation of ODE steps (indicated by markers) and correction steps C for  $2\times$  super-resolution on CelebA comparing LPIPS  $\downarrow$  (top), SSIM  $\uparrow$  (middle) and PSNR  $\uparrow$  (bottom) to processing time  $\downarrow$ . ODE steps increase from left to right and represent 4, 8, 16, 32, 64, 128 and 256, respectively. For better visualization, ODE steps 4 and 8 when using C=0 are omitted. The circle indicates the selected hyperparameters. Time is per image and displayed on a logarithmic scale.

Time (s)

each considered method are shown for the CelebA dataset in Fig. 4, for the AFHQ-Cat dataset in Fig. 1 (left) and also in the supplemental material. Ablations of hyperparameters are presented in Fig. 5.

Quantitative Results. Our evaluation on the CelebA dataset in Tab. 1 shows that Restora-Flow consistently outperforms all other flow-based methods in terms of perceptual quality, achieving the best LPIPS scores across all tasks. Moreover, our method achieves superior SSIM and PSNR distortion scores for denoising and super-resolution, while being a close second to Flow-Priors for box inpainting and to PnP-Flow for random inpainting. Further, it can be observed that diffusion-based RePaint delivers very competitive results in inpainting and super-resolution, while DDNM<sup>+</sup> performs well on box inpainting. Nevertheless, our Restora-Flow method is roughly 10× faster than RePaint and 6× faster than DDNM<sup>+</sup>, while delivering the same or even better reconstructions in terms of restoration quality. Additionally, when assessing quality scores and processing

times simultaneously, the plots in Fig. 4 clearly illustrate the benefits of Restora-Flow compared with all other studied methods across all tasks.

The superior performance of Restora-Flow in comparison with related work can also be observed on the other two natural image datasets considered in our evaluation, which confirms the versatility of our approach. On the AFHQ-Cat and COCO datasets, which differ strongly in terms of variety of the images to reconstruct, Restora-Flow outperforms all other flow-based methods in the perceptual LPIPS metric for all tasks except for super-resolution on AFHQ-Cat and for box inpainting on COCO. However, in both cases our results are a close second to the respective best performing method. Moreover, when looking at the other metrics over these datasets, we also achieve the best results in all metrics and closely match the best performing method for PSNR on AFHQ-Cat. Importantly, these great results were achieved in tandem with the fastest processing times in most settings. OT-ODE is the only related work that was able to be faster in two settings on AFHQ-Cat, however, it achieved inferior reconstruction quality in both cases. For diffusion-based baselines, we observe similar behavior as for CelebA, often delivering competitive results but at a significantly higher computational cost. The relationship between perceptual quality scores and processing times for AFHQ-Cat is visualized in Fig. 1, further demonstrating the advantages of our method compared to related work. For additional plots on AFHQ-Cat using distortion metrics, see suppl. material.

To further assess the versatility of our method, and to additionally study the dependence of the Restora-Flow algorithm on the specific implementation framework, we performed an experiment on a medical X-ray Hand dataset and integrated all baselines and our proposed method in the Med-DDPM framework (see Sec. 4). In-line with previously discussed results, our method consistently achieved great results for LPIPS, SSIM and PSNR compared with the baselines in a fraction of the time, see Tab. 1. The same behavior was also observed in the clinically motivated occlusion removal task, where downstream segmentation or classification tasks may benefit from imaging artifacts or anomalies being removed. Consistent with the other experiments, Restora-Flow achieved improved perceptual quality scores at lower processing times.

**Ablation.** Fig. 5 investigates the influence of ODE steps and correction steps C for  $2\times$  super-resolution on CelebA shown for LPIPS (top) and PSNR (bottom). ODE steps (indicated by markers) increase from left to right from 4 up to 256 for each C. As expected, more correction steps lead to longer evaluation times using the same number of ODE steps. Both graphs show a trade-off between fast sampling and better scores, with lower correction steps being advantageous despite requiring a larger number of ODE steps un-



Figure 6. Qualitative results on AFHQ-Cat. Shown are the degraded image (col 1), original image (col 2), restored images using related work as indicated (cols 3-8) and restored images of Restora-Flow (col 9). Rows refer to denoising (row 1), box inpainting (row 2), superresolution (row 3) and random inpainting (row 4). Differences can be best seen in the pdf version.

til the metrics saturate. Therefore, by setting C=1 for all experiments, the only hyperparameter that remains is the number of ODE steps, as in standard flow matching.

Qualitative Results. The qualitative results in Fig. 3, Fig. 6 and Suppl. Fig. 1 indicate notable differences in performance across different tasks and datasets among the studied baseline methods. OT-ODE tends to produce artifacts, particularly evident in box inpainting outputs on the CelebA and AFHQ-Cat datasets, as well as in the random inpainting task on the COCO dataset. Similarly, Flow-Priors generates noisy reconstructions in super-resolution outputs on the CelebA dataset, and produces artifacts in both super-resolution and random inpainting tasks on the AFHQ-Cat and COCO datasets, respectively. While D-Flow generally yields realistic results, it suffers from slow processing times and struggles to reconstruct certain objects for denoising on the COCO dataset. Despite achieving high SSIM and PSNR scores, PnP-Flow often produces oversmoothed results across all datasets. Among the diffusionbased baselines, DDNM+ tends to introduce artifacts in super-resolution tasks, while RePaint produces visually realistic results but at the expense of very slow processing. In contrast, our method was able to generate artifact-free and realistic images that maintain texture while ensuring fast processing across conducted experiments (see also Fig. 1). Additional examples are in the supplemental material.

For the medical dataset, (see Fig. 1 and Suppl. Fig. 3),

we observe lower overall variability among methods, likely due to the smaller variations present in hand X-ray images compared with natural images. Nonetheless, notable differences, which may be clinically significant due to anatomical changes, are evident in some tasks. For example, although D-Flow reconstructions initially appear realistic, the known input regions are often altered substantially (*e.g.*, in box inpainting), likely due to sensitive hyperparameters. In addition, several baselines struggle in the occlusion removal task, where occlusions remain partially visible in the reconstructed images. In contrast, our method consistently produces high-quality reconstructions across all tasks, with considerably faster processing times.

#### 6. Conclusion

We have introduced Restora-Flow, a flow matching-based algorithm designed for mask-guided image restoration. By effectively incorporating a trajectory correction mechanism within the mask-guided generation of a flow prior, our method has shown superior perceptual quality and reduced processing time across various tasks and datasets when compared to diffusion and flow-based baselines. Moreover, Restora-Flow requires no additional hyperparameters beyond the number of ODE steps utilized in standard flow matching. In future work, we plan to extend the algorithm to tackle image restoration tasks that involve non mask-based degradation operators.

# Acknowledgements

We would like to thank Mateusz Kozinski for constructive discussions and feedback that contributed to this work. This research was funded in whole or in part by the Austrian Science Fund (FWF) 10.55776/PAT1748423.

## References

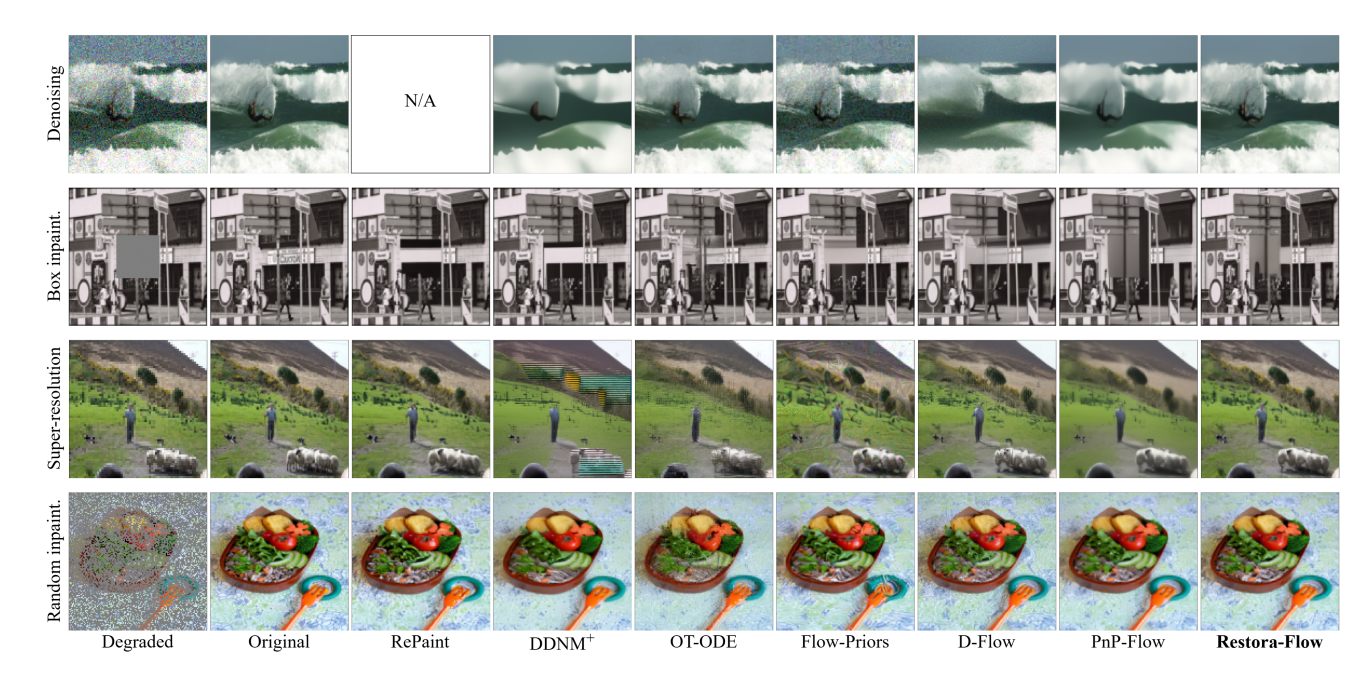
- [1] Grigory Bartosh, Dmitry P Vetrov, and Christian Andersson Naesseth. Neural flow diffusion models: Learnable forward process for improved diffusion modelling. In *Advances in Neural Information Processing Systems (NeurIPS)*, pages 73952–73985, 2025. arxiv: abs/2404.12940. 2
- [2] Heli Ben-Hamu, Omri Puny, Itai Gat, Brian Karrer, Uriel Singer, and Yaron Lipman. D-Flow: Differentiating through flows for controlled generation. In *International Conference on Machine Learning (ICML)*, 2024. arxiv: abs/2402.14017. 1, 2, 4, 5, 6
- [3] Yochai Blau and Tomer Michaeli. The perception-distortion tradeoff. In *IEEE/CVF Conference on Computer Vision and Pattern Recognition (CVPR)*, pages 6228–6237, 2018. doi: 10.1109/cvpr.2018.00652. 5
- [4] Lea Bogensperger, Dominik Narnhofer, Alexander Falk, Konrad Schindler, and Thomas Pock. FlowSDF: Flow matching for medical image segmentation using distance transforms. *International Journal of Computer Vision*, 133 (7):4864–4876, 2025. doi: 10.1007/s11263-025-02373-y. 2
- [5] Yunjey Choi, Youngjung Uh, Jaejun Yoo, and Jung-Woo Ha. StarGAN v2: Diverse image synthesis for multiple domains. In *IEEE/CVF Conference on Computer Vision and Pattern Recognition (CVPR)*, pages 8188–8197, 2020. doi: 10.1109/cvpr42600.2020.00821. 4
- [6] Hyungjin Chung, Jeongsol Kim, Michael Thompson Mccann, Marc Louis Klasky, and Jong Chul Ye. Diffusion Posterior Sampling for General Noisy Inverse Problems. In *In*ternational Conference on Learning Representations (ICLR), 2023. arxiv: abs/2209.14687. 2
- [7] Giannis Daras, Hyungjin Chung, Chieh-Hsin Lai, Yuki Mitsufuji, Jong Chul Ye, Peyman Milanfar, Alexandros G Dimakis, and Mauricio Delbracio. A survey on diffusion models for inverse problems. arXiv:2410.00083, 2024. arxiv: abs/2410.00083, 2
- [8] Prafulla Dhariwal and Alexander Nichol. Diffusion models beat GANs on image synthesis. In Advances in Neural Information Processing Systems (NeurIPS), pages 8780–8794, 2021. arxiv: abs/2105.05233. 2
- [9] Chao Dong, Chen Change Loy, Kaiming He, and Xiaoou Tang. Image super-resolution using deep convolutional networks. *IEEE Transactions on Pattern Analysis and Machine Intelligence (PAMI)*, 38(2):295–307, 2016. doi: 10.1109/TPAMI.2015.2439281. 2
- [10] Zolnamar Dorjsembe, Hsing-Kuo Pao, Sodtavilan Odonchimed, and Furen Xiao. Conditional diffusion models for semantic 3D brain MRI synthesis. *IEEE Journal* of Biomedical and Health Informatics, 28(7):4084–4093, 2024. doi: 10.1109/JBHI.2024.3385504. 6

- [11] Bradley Efron. Tweedie's formula and selection bias. *Journal of the American Statistical Association*, 106(496):1602–1614, 2011. doi: 10.1198/jasa.2011.tm11181. 2
- [12] Patrick Esser, Sumith Kulal, Andreas Blattmann, Rahim Entezari, Jonas Müller, Harry Saini, Yam Levi, Dominik Lorenz, Axel Sauer, Frederic Boesel, et al. Scaling rectified flow transformers for high-resolution image synthesis. In *International Conference on Machine Learning (ICML)*, 2024. arxiv: abs/2403.03206. 2
- [13] Arkadiusz Gertych, Aifeng Zhang, James Sayre, Sylwia Pospiech-Kurkowska, and HK Huang. Bone age assessment of children using a digital hand atlas. *Computerized Medical Imaging and Graphics*, 31(4-5):322–331, 2007. doi: 10.1016/j.compmedimag.2007.02.012. 4
- [14] Arnela Hadzic, Lea Bogensperger, Andrea Berghold, and Martin Urschler. Flow Matching-Based Data Synthesis for Robust Anatomical Landmark Localization. *IEEE Journal* of Biomedical and Health Informatics, page in press, 2025. doi: 10.1109/JBHI.2025.3603907. 4, 6
- [15] Jonathan Ho, Ajay Jain, and Pieter Abbeel. Denoising diffusion probabilistic models. In *Advances in Neural Information Processing Systems (NeurIPS)*, pages 6840–6851, 2020. arxiv: abs/2006.11239. 2
- [16] Ajil Jalal, Marius Arvinte, Giannis Daras, Eric Price, Alexandros G Dimakis, and Jon Tamir. Robust compressed sensing MRI with deep generative priors. In *Advances in Neural Information Processing Systems (NeurIPS)*, pages 14938–14954, 2021. arxiv: abs/2108.01368, 2
- [17] Bahjat Kawar, Gregory Vaksman, and Michael Elad. SNIPS: Solving noisy inverse problems stochastically. In *Advances in Neural Information Processing Systems (NeurIPS)*, pages 21757–21769, 2021. arxiv: abs/2105.14951. 2
- [18] Bahjat Kawar, Michael Elad, Stefano Ermon, and Jiaming Song. Denoising diffusion restoration models. In *Advances in Neural Information Processing Systems (NeurIPS)*, pages 23593–23606, 2022. arxiv: abs/2201.11793. 2
- [19] Tsung-Yi Lin, Michael Maire, Serge Belongie, James Hays, Pietro Perona, Deva Ramanan, Piotr Dollár, and C Lawrence Zitnick. Microsoft COCO: Common objects in context. In European Conference on Computer Vision (ECCV), pages 740–755, 2014. doi: 10.1007/978-3-319-10602-1\_48. 4
- [20] Yaron Lipman, Ricky TQ Chen, Heli Ben-Hamu, Maximilian Nickel, and Matt Le. Flow matching for generative modeling. In *International Conference on Learning Representations (ICLR)*, 2022. arxiv: abs/2210.02747. 2, 3
- [21] Xingchao Liu, Chengyue Gong, and Qiang Liu. Flow Straight and Fast: Learning to Generate and Transfer Data with Rectified Flow. In *International Conference on Learn*ing Representations (ICLR), 2023. arxiv: abs/2209.03003. 2, 3
- [22] Ziwei Liu, Ping Luo, Xiaogang Wang, and Xiaoou Tang. Deep Learning Face Attributes in the Wild. In *International Conference on Computer Vision (ICCV)*, 2015. doi: 10.1109/jccv.2015.425.4
- [23] Andreas Lugmayr, Martin Danelljan, Andres Romero, Fisher Yu, Radu Timofte, and Luc Van Gool. RePaint: Inpainting using denoising diffusion probabilistic models.

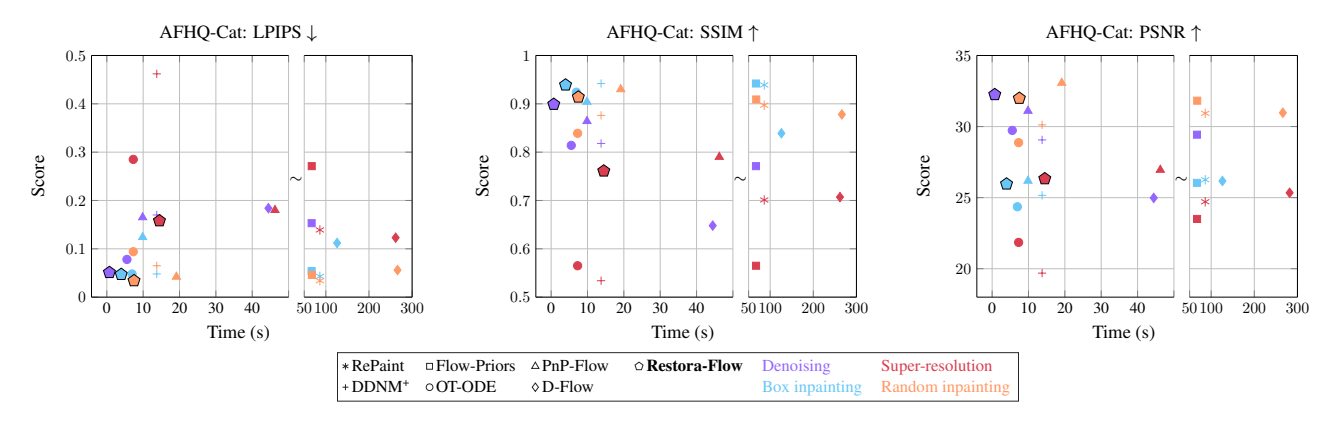
- In *IEEE/CVF Conference on Computer Vision and Pattern Recognition (CVPR)*, pages 11461–11471, 2022. doi: 10.1109/CVPR52688.2022.01117. 1, 2, 3, 5, 6
- [24] Morteza Mardani, Jiaming Song, Jan Kautz, and Arash Vahdat. A Variational Perspective on Solving Inverse Problems with Diffusion Models. In *International Conference on Learning Representations (ICLR)*, 2024. arxiv: abs/2305.04391. 2
- [25] Ségolène Tiffany Martin, Anne Gagneux, Paul Hagemann, and Gabriele Steidl. PnP-Flow: Plug-and-Play Image Restoration with Flow Matching. In *International Conference on Learning Representations (ICLR)*, 2025. arxiv: abs/2410.02423. 1, 2, 4, 5, 6
- [26] Ashwini Pokle, Matthew J Muckley, Ricky TQ Chen, and Brian Karrer. Training-free linear image inverses via flows. *Transactions on Machine Learning Research (TMLR)*, 2024. arxiv: abs/2310.04432. 1, 2, 4, 5, 6
- [27] Robin Rombach, Andreas Blattmann, Dominik Lorenz, Patrick Esser, and Björn Ommer. High-resolution image synthesis with latent diffusion models. In IEEE/CVF Conference on Computer Vision and Pattern Recognition (CVPR), pages 10684–10695, 2022. doi: 10.1109/CVPR52688.2022.01042, 2
- [28] Jascha Sohl-Dickstein, Eric Weiss, Niru Maheswaranathan, and Surya Ganguli. Deep unsupervised learning using nonequilibrium thermodynamics. In *International Conference on Machine Learning (ICML)*, pages 2256–2265, 2015. arxiv: abs/1503.03585. 2
- [29] Jiaming Song, Arash Vahdat, Morteza Mardani, and Jan Kautz. Pseudoinverse-guided diffusion models for inverse problems. In *International Conference on Learning Representations (ICLR)*, 2023. 2
- [30] Yang Song, Liyue Shen, Lei Xing, and Stefano Ermon. Solving inverse problems in medical imaging with score-based generative models. In *International Conference on Learning Representations (ICLR)*, 2021. arxiv: abs/2111.08005.
- [31] Yang Song, Jascha Sohl-Dickstein, Diederik P Kingma, Abhishek Kumar, Stefano Ermon, and Ben Poole. Score-Based Generative Modeling through Stochastic Differential Equations. In *International Conference on Learning Representations (ICLR)*, 2021. arxiv: abs/2011.13456. 2
- [32] Xin Tao, Hongyun Gao, Xiaoyong Shen, Jue Wang, and Jiaya Jia. Scale-recurrent network for deep image deblurring. In *IEEE/CVF Conference on Computer Vision and Pattern Recognition (CVPR)*, pages 8174–8182, 2018. doi: 10.1109/cvpr.2018.00853. 2
- [33] Singanallur V Venkatakrishnan, Charles A Bouman, and Brendt Wohlberg. Plug-and-play priors for model based reconstruction. In *IEEE Global Conference on Signal and Information Processing (GlobalSIP)*, pages 945–948, 2013. doi: 10.1109/globalsip.2013.6737048. 2
- [34] Yinhuai Wang, Jiwen Yu, and Jian Zhang. Zero-Shot Image Restoration Using Denoising Diffusion Null-Space Model. In *International Conference on Learning Representations* (ICLR), 2023. arxiv: abs/2212.00490. 1, 2, 5, 6
- [35] Syed Waqas Zamir, Aditya Arora, Salman Khan, Munawar Hayat, Fahad Shahbaz Khan, Ming-Hsuan Yang,

- and Ling Shao. Multi-stage progressive image restoration. In *IEEE/CVF Conference on Computer Vision and Pattern Recognition (CVPR)*, pages 14821–14831, 2021. doi: 10.1109/cvpr46437.2021.01458. 2
- [36] Aifeng Zhang, James W Sayre, Linda Vachon, Brent J Liu, and HK Huang. Racial differences in growth patterns of children assessed on the basis of bone age. *Radiology*, 250(1): 228–235, 2009. doi: 10.1148/radiol.2493080468. 4
- [37] Daikun Zhang, Qiuyi Han, Yuzhu Xiong, and Hongwei Du. Mutli-modal straight flow matching for accelerated MR imaging. *Computers in Biology and Medicine*, page 108668, 2024. doi: 10.1016/j.compbiomed.2024.108668.
- [38] Kai Zhang, Wangmeng Zuo, Shuhang Gu, and Lei Zhang. Learning deep CNN denoiser prior for image restoration. In *IEEE/CVF Conference on Computer Vision and Pattern Recognition (CVPR)*, pages 3929–3938, 2017. doi: 10.1109/cvpr.2017.300. 2
- [39] Richard Zhang, Phillip Isola, Alexei A Efros, Eli Shechtman, and Oliver Wang. The unreasonable effectiveness of deep features as a perceptual metric. In *IEEE/CVF Conference* on Computer Vision and Pattern Recognition (CVPR), pages 586–595, 2018. doi: 10.1109/cvpr.2018.00068. 5
- [40] Yasi Zhang, Peiyu Yu, Yaxuan Zhu, Yingshan Chang, Feng Gao, Ying Nian Wu, and Oscar Leong. Flow Priors for Linear Inverse Problems via Iterative Corrupted Trajectory Matching. In Advances in Neural Information Processing Systems (NeurIPS), 2024. arxiv: abs/2405.18816. 1, 2, 4, 5, 6
- [41] Yuanzhi Zhu, Kai Zhang, Jingyun Liang, Jiezhang Cao, Bihan Wen, Radu Timofte, and Luc Van Gool. Denoising diffusion models for plug-and-play image restoration. In *IEEE/CVF Conference on Computer Vision and Pattern Recognition Workshops (CVPRW)*, pages 1219–1229, 2023. doi: 10.1109/CVPRW59228.2023.00129. 2

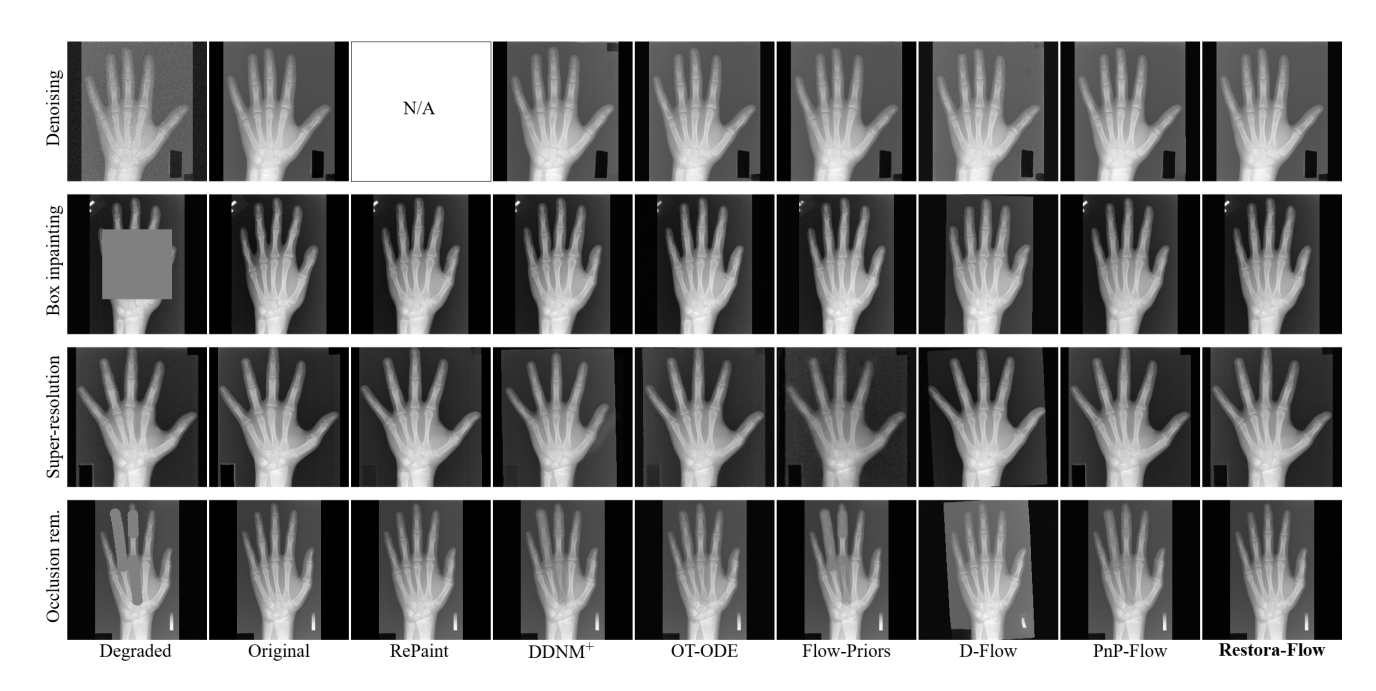
# **Appendix**



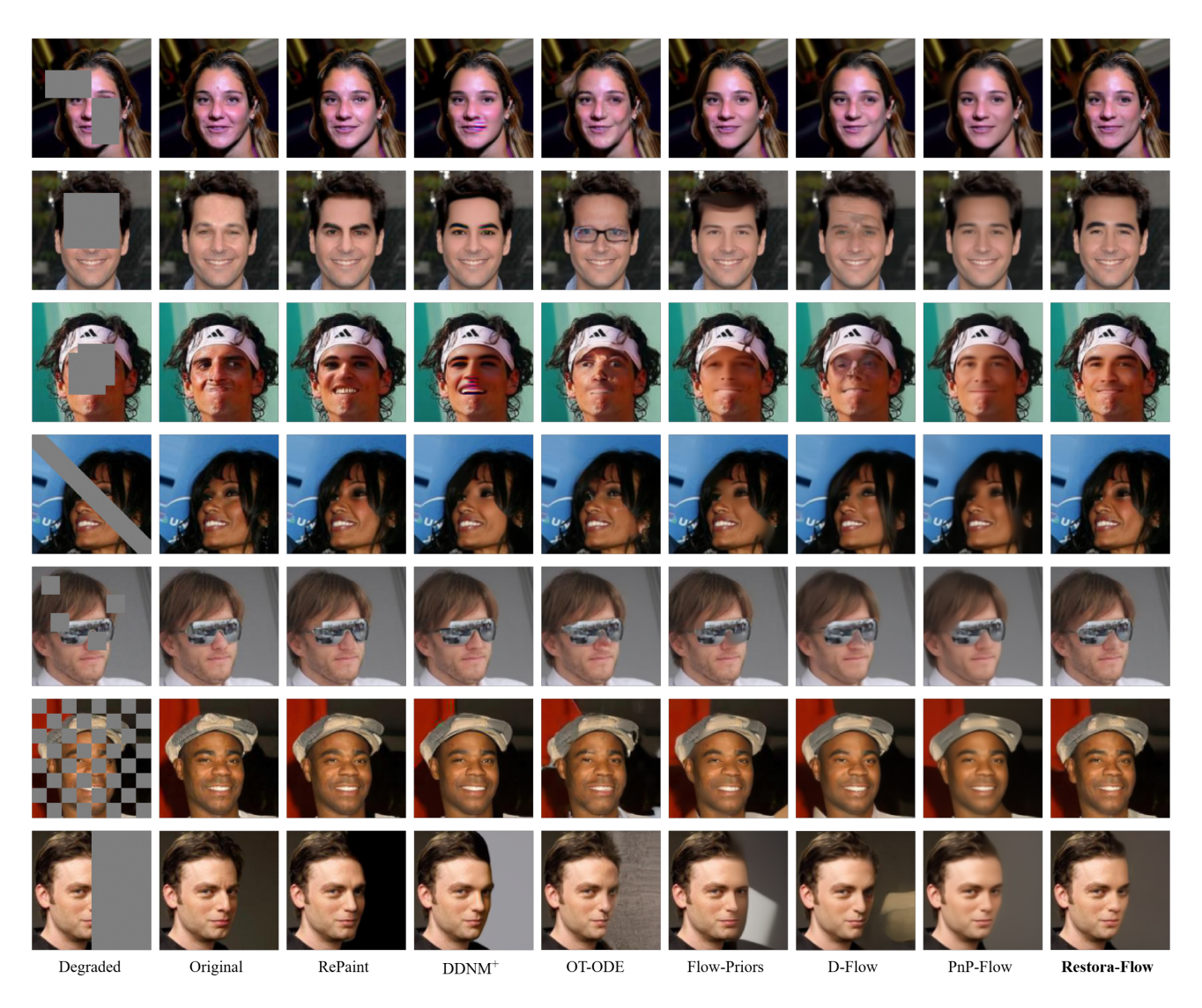
Supplemental Figure 7. Qualitative results on COCO. Shown are the degraded image (col 1), original image (col 2), restored images using related work as indicated (cols 3-8) and restored images of Restora-Flow (col 9). Rows refer to denoising (row 1), box inpainting (row 2), super-resolution (row 3) and random inpainting (row 4). Differences can be best seen in the pdf version.



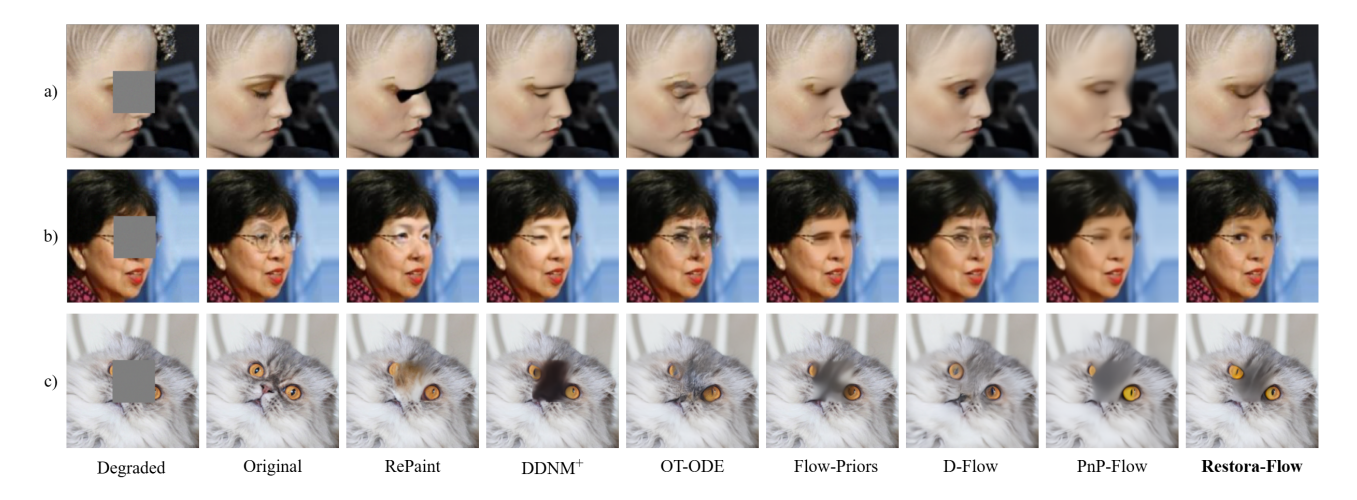
Supplemental Figure 8. Visual representation of quantitative results on CelebA. Restora-Flow  $(\bigcirc)$  is compared to related work methods (other shapes) on four different tasks (colors). The plots represent LPIPS  $\downarrow$  (left), SSIM  $\uparrow$  (center) and PSNR  $\uparrow$  (right) on the y-axis, and processing time  $\downarrow$  (all plots) on the x-axis. For better visualization and comparison, each plot is separated into two parts with different scales in the x-axis.



Supplemental Figure 9. Qualitative results on X-ray Hand. Shown are the degraded image (col 1), original image (col 2), restored images using related work as indicated (cols 3-8) and restored images of Restora-Flow (col 9). Rows refer to different tasks as indicated. RePaint is not applicable to denoising (N/A).



Supplemental Figure 10. Qualitative comparison of image restoration methods on CelebA using various input masks. Differences can be best seen in the pdf version.



Supplemental Figure 11. Representative failure cases of Restora-Flow and comparison methods. (a) A face in profile view, deviating from the typically front-facing images in CelebA. (b) An example with occlusion due to glasses (CelebA). (c) An atypical AFHQ-Cat image where the cat's appearance differs from typical samples in the dataset (*e.g.*, ears not visible).